EasyChair Preprint

№ 13825

Bond Strength of Lap Spliced High-Modulus GFRP Bars in Concrete: an Experimental Evaluation and Design Codes Assessment

Seyed Arman Hosseini, Ahmed Sabry Farghaly, Abolfazl Eslami and Brahim Benmokrane

July 5, 2024

Bond Strength of Lap Spliced High-Modulus GFRP Bars in Concrete: An Experimental Evaluation and Design Codes Assessment

Seyed Arman Hosseini[1,2], Ahmed Sabry Farghaly[1], Abolfazl Eslami[1], Brahim Benmokrane[1]

[1] Department of Civil and Environmental Engineering, Faculty of Engineering, University of Sherbrooke, Sherbrooke, Quebec, Canada J1K 2R1.
[2] **Corresponding Author:** seyed.arman.hosseini.ghahroudi@usherbrooke.ca

Abstract. Lap splicing is the most common and cost-efficient method for connecting bars in GFRP-reinforced concrete structures. However, there is a lack of knowledge regarding the bond behavior of high-modulus GFRP bars in concrete. The present study aims to fill this gap by investigating the bond strength of lap-spliced high-modulus GFRP bars in concrete. These new-generation GFRP bars have a modulus of elasticity of up to 65 GPa and an ultimate tensile strength of up to 1400 MPa. Three large−scale splice beam tests, with a rectangular cross-section of 300 mm × 450 mm and a length of 5,200 mm, varying splice lengths ($28d_b$, $38d_b$, and $45d_b$), were designed to evaluate predictions of bond strength for North American design codes. Results show a nonlinear decrease in bond strength by 14.7% and 17.7% with a 36% and 60% increase in splice length, attributed to uneven bond stress distribution. On the other hand, these increases in splice length led to an increase in the splice strength by 17.7% and 31.8%, respectively. ACI 440.11-22 provides the most accurate predictions, showing an average test-to-prediction ratio of 1.03, while CSA S806-12 and CSA S6-19 overestimate with average test-to-prediction ratios of 0.84 and 0.57, respectively. In the latest Canadian Highway Bridge Design Code (CSA S6-25), the revised factor for GFRP-to-steel bond strength improves predictions with a test-to-prediction ratio of 0.89. However, Canadian codes generally over-predict bond strength, particularly by increasing the splice length to bar diameter ratio, neglecting the nonlinear bond stress distribution along the embedment length.

Keywords: Lap splicing, Bond strength, Splice strength, Development length, Splice length, High modulus GFRP bars.

1 Introduction

Concerns about the durability of reinforced concrete structures, affecting both new and existing buildings, arise from the significant issue of steel bar corrosion. Influenced by factors like road de-icing salt, and harsh climate conditions, this corrosion leads to weakened concrete elements, causing cracking and structural failure in various components. The resulting repair costs run into billions of dollars from public funds [1-3]. A promising solution involves replacing steel bars with glass fiber-reinforced polymer (GFRP) bars, known for exceptional corrosion resistance and a high stiffness-to-weight ratio, promoting environmental sustainability and long-lasting construction [2-4].

While GFRP bars offer numerous advantages, they do have a lower modulus of elasticity and exhibit weaker bond strength to concrete compared to steel bars. Consequently, understanding the bond behavior of GFRP bars in concrete is crucial for assessing the performance of GFRP-reinforced concrete members, as it governs the serviceability and cracking behavior of such structures. Hence, studying the bond behavior of the latest generation of GFRP bars with improved mechanical properties is essential for updating design codes. This, in turn, enhances the feasibility of substituting steel bars with GFRP bars in concrete infrastructure projects and capitalizing on their superior characteristics [4-6].

Limited research has been conducted on the bond behavior of the latest generation of GFRP bars. The current assessment of their bond strength in concrete, according to Canadian and American design standards, relies on outdated test data from over two decades ago, using GFRP bars no longer commercially available. Advances in the mechanical properties and manufacturing techniques of the new generation of GFRP bars underscore the need for further investigation into their bond behavior in concrete structures [6-12]. This new generation of GFRP bars has a higher modulus of elasticity (more than 60 GPa) and tensile strength (more than 1200 MPa) and benefits from improved surface treatments that enhance their bond with concrete.

Different test methods can be employed to assess the bond strength of GFRP bars in concrete, including pull-out tests, beam-end tests, notch-beam tests, and splice-beam tests. Among these, the splice-beam test provides the most realistic values for the bond strength of GFRP bars in flexural members [7-9]. Additionally, valuable data can be collected through the splice-beam test to estimate the required splice length for GFRP bars. This is particularly important since lap splicing of GFRP bars is inevitable in construction, as a common method for connecting bars [4,7-9]. The primary objective of the present research paper is to acquire experimental data that enhances our understanding of the bond strength of high-modulus GFRP bars and to compare the estimation of bond strength given by current North American design codes with experimental results.

The present research specifically investigates the effect of varying embedment length on the bond strength of GFRP bars in concrete through conducting three large−scale splice beam tests with splice lengths of 28, 38, and 45 times the bar diameter. The study evaluates parameters such as the load-deflection relationship, failure mode, and bond strength. Additionally, it analyzes the accuracy of design codes—ACI 440.11-22, CSA S6-19, CSA S806-12, and CSA S6-25—in predicting the bond strength of lap-spliced GFRP bars, comparing them with the test results. Through this investigation, the research aims to advance knowledge regarding the bond behavior of GFRP bars in concrete, ultimately enhancing the design and application of GFRP bars in concrete structures.

2 Experimental Program

2.1. Material Properties

All three beams were cast using ready-mix concrete with a maximum aggregate size of 16 mm (0.63 in.). For compressive strength evaluation, five standard concrete cylinders of 150

× 300 mm (5.9 × 11.8 in.) were prepared for each beam following ASTM C39 [19] guidelines. The measured average compressive strengths of the concrete at 28 days and during beam testing ranged between 38.3 and 41.9 MPa (5.55 and 6.08 ksi), as detailed in Table 1. Longitudinal reinforcement was achieved using M16 (No.5) sand-coated grade III GFRP rebar, with a nominal diameter of 15.9 mm (0.62 in.), and area of 200 mm² (0.31 in.²) according to ASTM D8505 [20]. Furthermore, bars used in this study have measured diameter of 17.2 mm (0.68 in.), and area of 238 mm² (0.37 in.²) which are used for further calculations. The measured average tensile strength and modulus of elasticity for No. 5 GFRP bars are 1,428 MPa (207.1 ksi) and 65.4 GPa (9,485.5 ksi) as per ASTM 7205 [21], respectively. GFRP M13 (No.4) stirrups were employed as transverse reinforcement throughout the shear spans, while two M13 (No.4) GFRP bars were also used to support stirrups during cage construction and for handling purposes after failure.

2.2. Specification of Test Specimens

Figures 1 and 2 provide details of the test specimens, comprising three beams with a rectangular cross-section measuring 300 × 450 mm (11.8 × 17.7 in.), an overall length of 5,200 mm (204.7 in.), and an effective span of 4,800 mm (189.0 in.). The constant moment zone spans 2,500 mm (98.4 in.), with two shear spans of 1,150 mm (45.3 in.). No shear stirrups were used in the constant moment region for any of the specimens.

The shear design of the beams followed ACI 440.11-22 [13] and was based on the ultimate flexural capacity of the beam with continuous bars to prevent shear failure before lap splice failure. Two shear spans were reinforced using 12 mm (0.47 in.) diameter GFRP stirrups spaced at 100 mm (3.94 in.) center-to-center. The design also considered the configuration of the side and bottom concrete cover of the spliced bars, as well as the clear bar spacing. The side clear concrete cover to bars was set at 55 mm, while the bottom clear concrete cover was established at 38 mm. The required splice length proposed by ACI 440.11-22 can be calculated using the development length (l_d) equation, considering the splice length equal to $1.0l_d$, resulting in 103 times the bar diameter.

To ensure splice failure before reaching the ultimate capacity of beams in flexure, the specimens were reinforced with GFRP splices measuring 28, 38, and 45 times the nominal bar diameter, corresponding to 450, 610, and 720 mm (17.7, 24.0, and 28.3 in.), respectively. Figure 1 depicts the reinforcement details within the constant-moment region of beams with lap splice lengths of $28d_b$, $38d_b$, and $45d_b$. A two-part notation is used to represent the variables in each beam, signifying the GFRP bar size (No. 5) and the splice length in millimeters: L450, L610, and L720 for beams with splice lengths 28, 38, and 45 times the bar diameter, respectively.

2.3. Instrumentation and Test Setup

All beams underwent a four-point bending test, as shown in Figure 2. A 1000 kN (225 kip) MTS actuator applied the load at a displacement rate of 1.2 mm/min until failure. Mid-span deflection was continuously monitored using linear variable differential transformers (LVDTs) at mid-span and load application points on the bottom face of the beam. Strain

values in both the reinforcing bars and concrete were recorded during loading using electrical strain gauges. Before casting, two strain gauges (SG1 and SG2) were installed at both ends of one of the splices on the GFRP bars, and the other two (SG3 and SG4) were placed in the middle of both splices on the GFRP bars. To protect the strain gauges, those outside the splice regions were mounted 20 mm away from the splice ends. The positions of strain gauges on GFRP bars and the concrete surface are illustrated in Figures 1 and 2, respectively. Additionally, crack width evolution up to failure was monitored for two main flexural cracks located at the ends of splices using two LVDTs installed perpendicular to the cracks. Other flexural cracks within the span were visually checked during loading.

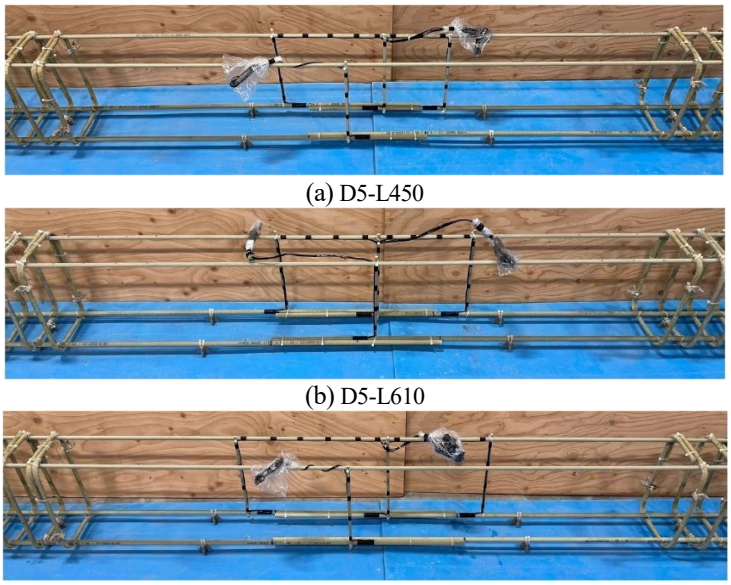

(a) D5-L450

(b) D5-L610

(c) D5-L720

Fig. 1. Reinforcement arrangement of lap spliced beams with different splice lengths (Note: 1 mm = 0.0394 in.).

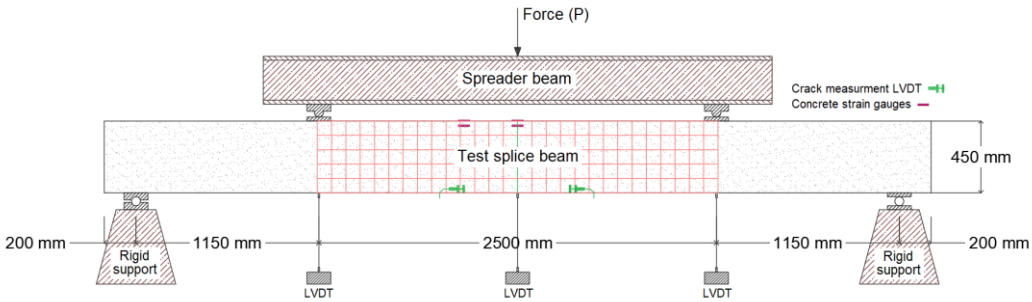

Fig. 2. Schematic illustration and overview of the test setup (Note: 1 mm = 0.0394 in.).

3 Test Results

3.1. Load-Deflection Behavior and Failure Modes

Figure 3 presents the load versus mid-span deflection distribution for all beams. The load-deflection responses exhibit a distinct bilinear pattern, indicating a reduction in flexural stiffness due to concrete cracking. Minor variations in cracking loads may be attributed to slight differences in concrete tensile strength of specimens. Notably, all beams maintained consistent stiffness levels before and after cracking, indicating unchanged axial stiffness in the longitudinal spliced bars, irrespective of the splice length. The results clearly demonstrate that increasing the splice length by 36% (from $28d_b$ to $38d_b$) and 60% (from $28d_b$ to $45d_b$) led to a respective 13.9% and 28.6% increase in ultimate load-carrying capacity, respectively.

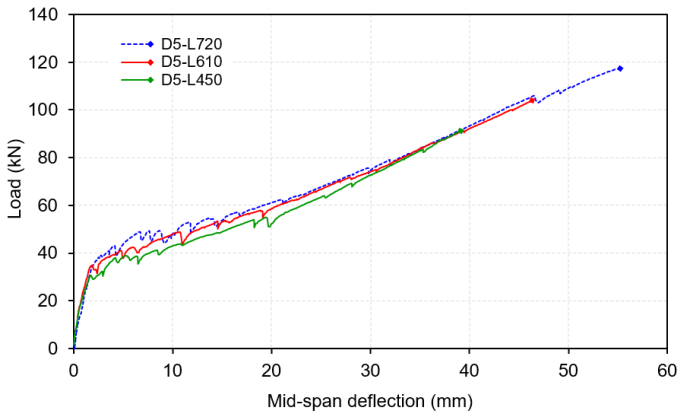

Fig. 3. Load–deflection responses of specimens splice lengths of $28d_b$, $38d_b$, and $45d_b$ (Note: 1 mm = 0.0394 in.; 1 kN = 0.2248 kips).

During the tests, initial flexural cracks appeared within the constant-moment region, typically outside the splice zone. The first flexural crack within the splice zone typically occurred at the splice ends. As the load neared failure, the number of flexural cracks within the constant-moment region increased. At higher loads, hairline splitting cracks initiated from the flexural crack near the splice end and gradually propagated within the splice zone on the bottom face of the beams, particularly near failure loads.

Figures 4(a) to 4(c) depict the observed failure modes of representative specimens with splice lengths of 450 mm ($28d_b$), 610 mm ($38d_b$), and 720 mm ($45d_b$), respectively. As initially designed, the failure of all beams was accompanied by the sudden splitting of the concrete cover in the spliced region. This splitting failure was explosive, the less the splice length was the more brittle failure was observed, leading to the peeling off of both bottom and side face of the beams for D5-L450 and D5-L610 beams, and just bottom face of D5-720 beam with no signs of bond splitting cracks on the sides of the beams up to the point of failure.

During loading, crack-width development was monitored with two LVDTs installed perpendicular to the two main cracks that appeared at the end of the splice region. The maximum crack width was determined by selecting the larger of the two measurements. Table 1 further provides a summary of maximum crack widths at failure for all test specimens. Based on the experimental observations, increasing the splice length by 36% (from $28d_b$ to $38d_b$) and 60% (from $28d_b$ to $45d_b$) resulted in an increase in the maximum crack width by 20.4% and 74.3%, respectively.

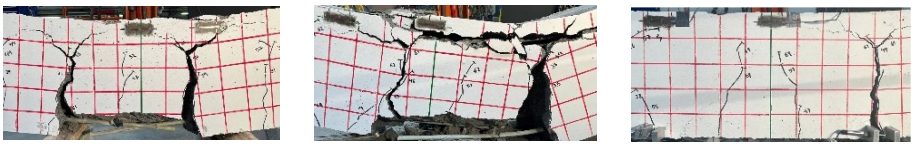

(a) D5-L450 (b) D5-L610 (c) D5-L720

Figure 4 – Observed failure modes of specimens.

3.2. Bond Strength

The calculation of bond stress in the rebar is challenging due to the complex distribution of bond stresses along its length. To address this, it's common practice to compute the average bond stress along the splice length. In this study, strain gauges were positioned at the splice ends to measure strain variations in the reinforcing bars. The mean maximum value of the measured strains (from SG1 and SG2) was taken as the failure strain of the reinforcement (ε_{test}). Multiplying this failure strain by the elastic modulus of the corresponding bars (E_f) resulted in the failure stress (f_{test}). This calculation, also referred to as splice strength, is detailed in Table 1. The average bond stress acting on the surface of spliced bars, denoted as $u_{avg.}$, and referred to as bond strength in this context, was then calculated by assuming that the tensile force applied to the rebar was counteracted by a uniform stress distribution across the entire surface of the rebar, as defined by:

$$u_{avg.} = \frac{f_{test}\, d_b}{4\, l_e} \tag{1}$$

To assess analytically predicted strain values for beams with spliced bars, experimental strain values were compared. In the analytical approach, the cracking load was determined using elastic flexural theory, considering it as the load where the stress in the extreme tension fiber equaled the modulus of rupture. Elastic load-deflection stiffness was assumed up to the cracking load, and a constant strain was used for the transition from the un-cracked to the cracked stage. After cracking, strain in the reinforcing bars at different loads was computed through moment-curvature analysis, utilizing the parabolic stress-strain relationship proposed by Todeschini [3]. Table 1 shows that theoretical values derived from moment-curvature analysis, confirmed by strain gauge measurements, have a maximum difference of 5% from measured strain values.

The bond stress on the surface of a reinforcing bars is directly related to the fourth root of the compressive strength of concrete [14]. To standardize values and account for variations in concrete compressive strength, all results were normalized by the fourth root of the compressive strengths divided by 40 MPa ($\sqrt[4]{f'_c/40}$ in SI units). As shown in Table 1, increasing the splice length led to an increase in the normalized splice strength ($f_{test,n}$). However, this relationship followed a nonlinear pattern, as observed in Figure 5. For instance, increasing the splice length from $28d_b$ to $38d_b$ (about 36%) and from $28d_b$ to $45d_b$ (a 60% increase) resulted in a 17.7% and 31.8% increase in splice strength, respectively. On the other hand, as depicted in Figure 5, with approximately 36% and 60% increases in splice length from $28d_b$ to $38d_b$ and $45d_b$, the bond strength ($u_{avg.}$) decreased by 14.7% and 17.7%, respectively. This behavior is also supported by previous studies [4,9,18] and can be attributed to the non-uniform distribution of bond stresses along the lap splice length, where a longer splice length increases splice strength but leads to lower bond strength levels.

Table 1. Summary of test results.

Specimen designation	Concrete compressive strength [28-day]	Measured values			Theoretical strain values	Normalized splice strength	Average bond strength	Maximum crack width at failure
	f'_c (MPa)	P_u (kN)	ε_{test} (με)	f_{test} (MPa)	$\varepsilon_{theo.}$ (με)	$f_{test,n}$ (MPa)	$u_{avg.}$ (MPa)	$w_{cr,max}$ (mm)
D5-L450	41.9	91.2	6291	412	6482	417	4.08	1.52
D5-L610	39.1	103.9	7411	485	7164	482	3.48	1.83
D5-L720	41.8	117.3	8289	543	7861	549	3.36	2.65

Note: 1 mm = 0.0394 in; 1 MPa = 0.145 ksi; 1 kN = 0.225 kips.

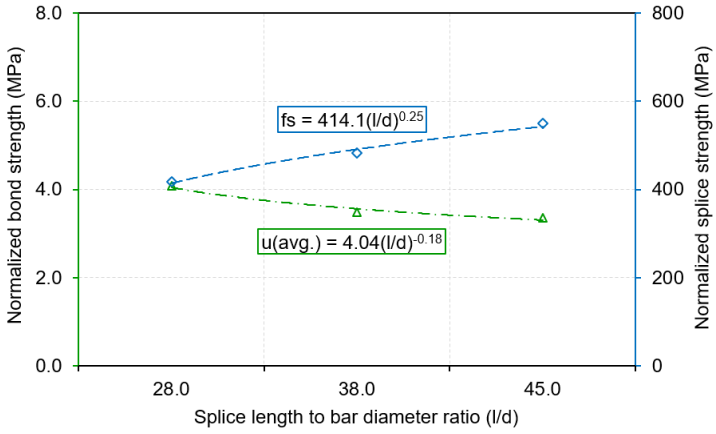

Fig. 4. Variation of average bond strength ($u_{avg.}$) and splice strength ($f_{test,n}$) with lap splice length (Note: 1 MPa = 0.145 ksi).

4 Design Codes Assessment

The experimental values of the average bond stress ($u_{test,n}$) acting on the surface of lapped bars, which is called bond strength in this context, collected in the present study have been compared with those calculated using expression provided by Wambeke and Shield [15], ACI 440.11-22 [13], CSA S6-19 [16], and CSA S806-12 [17], as depicted in Table 2. Except the direct expression proposed by Wambeke and Shield to calculate the bond strength, Eq. (2), other design codes recommend equations for calculating the development length of FRP bars and the amount of bond strength shall be calculated by solving Eq. (3) to Eq. (5) for the average bond stress developed on a given embedment length using Eq. (1). The direct expression given by Wambeke and Shield for calculating the bond strength of FRP bars is as follows [15]:

$$\frac{u}{0.083\sqrt{f'_c}} = 4.0 + 0.3\frac{c}{d_b} + 100\frac{d_b}{l_e} \tag{2}$$

It should be noted that the code recommendations in FRP reinforced concrete structures involve an incremental multiplier of 1.3 to replace the development length with the splice length, which is the same as the splice type factor in steel reinforced concrete design codes. This multiplier was not considered when calculating and comparing bond values provided by design codes with experimental results. This decision was based on the fact that bond strength expressions were primarily derived from end-beam, splice beam, and notch beam tests, and no distinction was made between different splice types and their corresponding multipliers provided by design codes. Furthermore, the accuracy of this hypothesis lacks support from experimental evidence. This gap could be addressed by investigating the influence of different splice types on the bond strength of lapped bars in future studies.

Table 2. Current design codes and guidelines for tension development length of FRP bars.

Design codes	Development length expressions†
ACI 440.11-22	$l_d = \dfrac{\alpha\dfrac{f_{fr}}{0.083\sqrt{f'_c}} - 340}{13.6 + \dfrac{c}{d_b}} \times d_b$ (3)
CSA S806-12	$l_d = 1.15\dfrac{k_1k_2k_3k_4k_5}{d_{cs}} \times \dfrac{f_{fr}}{\sqrt{f'_c}} \times A_b$ (4)
CSA S6-19	$l_d = 0.45\dfrac{k_1k_4}{d_{cs} + K_{tr}\dfrac{E_{frp}}{E_s}} \times \dfrac{f_{fr}}{f_{cr}} \times A_b$ where: $K_{tr} = \dfrac{A_{tr}f_y}{10.5sn}$ (5)
CSA S6-25	$l_d = 0.45\dfrac{k_1}{k_4[d_{cs} + K_{tr}\dfrac{E_{frp}}{E_s}]} \times \dfrac{f_{fr}}{f_{cr}} \times A_b$ where: $K_{tr} = 38.0\dfrac{A_{tr}}{sn}$ (6)

† SI units (MPa and mm)

Note: 1 mm = 0.0394 in; 1 MPa = 0.145 ksi; 1 kN = 0.225 kips.

Figure 6 shows that the bond strength values for D5-L450, D5-L610, and D5-L720 beams are overestimated using Eq. (2) proposed by Wambeke and Shield, with test-to-prediction ratios of 0.88, 0.88, and 0.87, respectively. Incorporating ACI 440.11-22, Eq. (3), for FRP bar bond strength calculation underestimates experimental values in beams with splice lengths of 450 mm ($28d_b$), 610 mm ($38d_b$), and 720 mm ($45d_b$), with test-to-prediction ratios of 1.04, 1.03, and 1.02, respectively.

The prediction of FRP lapped bar bond strength using Eq. (5) from CSA S806-12 in D5-L450, D5-L610, and D5-L720 beams results in overestimation, with test-to-prediction ratios of 0.94, 0.81, and 0.78, respectively. Additionally, CSA S6-19 overestimates bond strength considerably in beams with splice lengths of 450 mm ($28d_b$), 610 mm ($38d_b$), and 720 mm ($45d_b$), with test-to-prediction ratios of 0.63, 0.56, and 0.52, respectively. However, the updated CSA S6-25 provides more accurate predictions, with test-to-prediction ratios of 0.99, 0.87, and 0.82 for D5-L450, D5-L610, and D5-L720, respectively.

In Figure 6, it is evident that ACI 440.11-22 consistently predicts bond strength accurately across beams with varying splice lengths. In contrast, both Canadian design codes tend to over-predict experimental bond strength as splice length increases. This discrepancy may be attributed to the fact that CSA S806-12, CSA S6-19, and CSA S6-25 overlook the nonlinear distribution of bond stress along the embedment length, resulting in lower bond strengths for longer splice lengths, as supported by findings from other researchers [4,7,18].

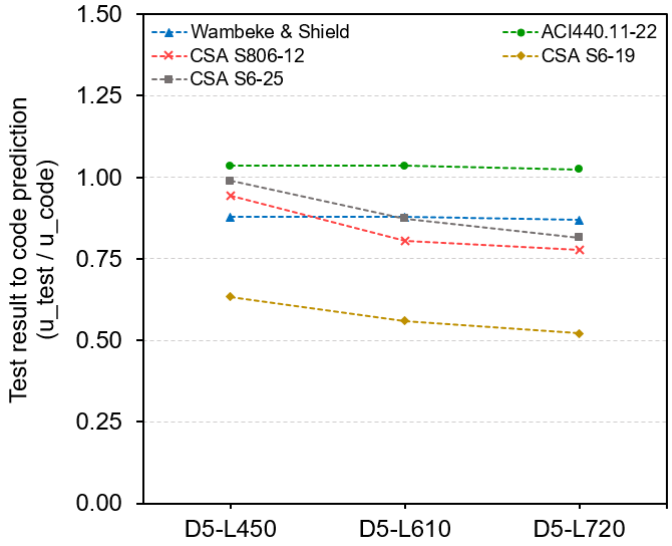

Fig. 5. Test results to code predictions ratio of bond strength of lap spliced GFRP bars
(Note: 1 MPa = 0.145 ksi.)

5 Summary and Conclusions

A total of three large–scale beam-splice tests were performed to assess the bond behavior of new generation GFRP bars with high modulus of elasticity in concrete. Based on the experimental findings, the following conclusion remarks can be drawn:

- Increasing splice length decreases bond strength and of new generation GFRP bars in lap spliced concrete members due to non-linear bond stress distribution.
- Longer splice lengths lead to an increase in splice strength, characterized by a non-linear relationship with a power exponent of 0.25.
- ACI 440.11-22 provides the most accurate predictions for bond strength, while CSA S806-12 and CSA S6-19 tend to overestimate, emphasizing the need for precise Canadian code provisions.
- The revised factor stands for GFRP-to-steel bond strength in the latest Canadian Highway Bridge Design Code (CSA S6-25) improves bond strength predictions.
- Canadian codes, despite improvements in CSA S6-25, over-predict bond strength, particularly when increasing splice length to bar diameter ratio, revealing a need for refining code provisions for these conditions.

Acknowledgements

This research was conducted with funding from the Tier-1 Canada Research Chair in Advanced Composite Materials for Civil Structures, the Natural Sciences and Engineering Research Council of Canada (NSERC), and the NSERC Industrial Research Chair in FRP Reinforcement for Concrete Infrastructure. The authors would like to thank the technical staff of the Canadian Foundation for Innovation (CFI) structural and materials lab in the Department of Civil Engineering at the University of Sherbrooke.

References

1. Apostolopoulos, C., & Papadakis, V. (2008). Consequences of steel corrosion on the ductility properties of reinforcement bar. Construction and Building Materials, 22(12), 2316–2324. https://doi.org/10.1016/j.conbuildmat.2007.10.006.
2. D'Antino, T., & Pisani, M. (2019). Long-term behavior of GFRP reinforcing bars. Composite Structures. https://doi.org/10.1016/J.COMPSTRUCT.2019.111283.
3. Todeschini, C. E., Bianchini, A. C. and Kesler, C. E. (1964). Behavior of Concrete Columns Reinforced with High-Strength Steels," Journal of the American Concrete Institute, Vol. 61, No.6.
4. Hosseini, S. A., Farghaly, A. S., Eslami, A., Nanni, A., & Benmokrane, B. (2024). Bond behaviour of lap spliced GFRP bars in concrete members: A state-of-the-art review and design recommendations. Construction and Building Materials, 411, 134714. https://doi.org/10.1016/j.conbuildmat.2023.134714.

5. Zemour, N., Asadian, A., Ahmed, E. A., Khayat, K. H., & Benmokrane, B. (2018). Experimental study on the bond behavior of GFRP bars in normal and self-consolidating concrete. Construction and Building Materials, 189, 869–881. https://doi.org/10.1016/j.conbuildmat.2018.09.045.
6. Yan F, Lin Z, Yang M. (2016). Bond mechanism and bond strength of GFRP bars to concrete: A review. Compos B Eng; 98:56–69. https://doi.org/10.1016/j.compositesb.2016.04.068.
7. Wu, C., Hwang, H.-J., & Ma, G. (2022). Effect of stirrups on the bond behavior of lap spliced GFRP bars in concrete beams. Engineering Structures, 266, 114552. https://doi.org/10.1016/j.engstruct.2022.114552.
8. Asadian, A., Eslami, A., Farghaly, A. S., & Benmokrane, B. (2019). Splice strength of staggered and non-staggered bundled glass fiber-reinforced polymer reinforcing bars in concrete. ACI Structural Journal, 116(4). https://doi.org/10.14359/51714482.
9. Y. Al-Salloum, L. Alaoud, H. Elsanadedy, A. Albidah, T. Almusallam, H. Abbas, Bond performance of GFRP Bar-splicing in reinforced concrete beams, J. Compos. Constr. 26 (2) (2022), https://doi.org/10.1061/(ASCE)CC.1943-5614.0001190.
10. Benmokrane, B., Mehany, S., Shield, C., Nanni, A., & Brown, V. L. (2023). Properties, longitudinal tensile properties, and bond strength of the new generation of GFRP bars. ASCE Journal of Composite for Construction, 27(6), 04023056.
11. Benmokrane, B., Mehany, S., Shield, C., Nanni, A., & Brown, V. L. (2023). Bond-dependent coefficient (kb) for new generation GFRP bars. ASCE Journal of Composite for Construction, 27(6), 04023057.
12. Benzecry, V., Ruiz Emparanza, A., De Casoy Basalo, F., & Nanni, A. (2021). Bond coefficient, kb, of GFRP bars. Construction and Building Materials, 292(123380).
13. ACI Committee 440 (2022). "Guide for the design and construction of structural concrete reinforced with fiber-reinforced polymer (FRP) bars (ACI 440.11-22)." American Concrete Institute, Farmington Hills, Michigan, USA.
14. ACI 408 Committee. (2003). Bond and Development of Straight Reinforcing Bars in Tension (ACI 408R-03). American Concrete Institute, Detroit, Michigan, US.
15. Wambeke, B. W., & Shield, C. K. (2006). Development length of glass fiber-reinforced polymer bars in concrete. ACI Structural Journal, 103(1), 11–17. https://doi.org/10.14359/15081.
16. Canadian Standards Association (2019). Canadian Highway Bridge Design Code (CAN/CSA S6-19). Canadian Standards Association, Ontario, Canada.
17. Canadian Standards Association (2012). Design and construction of building structures with fiber reinforced polymers (CAN/CSA S806-12). Canadian Standards Association, Ontario, Canada.
18. Makhmalbaf, E., & Razaqpur, A. G. (2021). Development length of glass fibre reinforced polymer (GFRP) rebar based on non-uniform bond stress, Canadian Journal of Civil Engineering. 49, 420–431. https://doi.org/10.1139/cjce-2020-0400.
19. ASTM Committee C09. “C39/C39M-21, Standard Test Method for Compressive Strength of Cylindrical Concrete Specimens,” ASTM International, West Conshohocken, PA. USA, 2021.
20. ASTM D8505/D8505M-23. “Standard Specification for Basalt and Glass Fiber Reinforced Polymer (FRP) Bars for Concrete Reinforcement,“ ASTM International, West Conshohocken, PA. USA, 2023.
21. ASTM D7205/D7205M-06. “Standard Test Method for Tensile Properties of Fiber Reinforced Polymer Matrix Composite Bars,“ ASTM International, West Conshohocken, PA. USA, 2006.